Optical absorption spectroscopy and properties of single walled carbon nanotubes at high temperature

Aljoscha Roch*, Lukas Stepien, Teja Roch, Ines Dani, Christoph Leyens, Oliver Jost, Andreas Leson

Fraunhofer Institute of Material and Beam Technology, Winterbergstr. 28, 01277 Dresden, Germany

ABSTRACT

Here, we present an experimental investigation of the optical spectra of single walled carbon nanotubes (SWCNT) at temperatures up to 1273 K. This investigation gives insights into the electronic structure of metallic and semiconducting SWCNT at different temperatures by measuring the shift of the S_{11}-, S_{22}- and M_{11}-band with optical absorption spectroscopy. We observed a decrease of the transition energies in both metallic and semiconducting SWCNT with increasing temperature determined by the shift of the S_{11}-, S_{22}- and M_{11}-absorption bands. The shifts follow the Varshni-equation. Furthermore, calculation of the average exciton binding energy (80–90 meV) in metallic SWCNT from the shift of the M_{11}-band was performed. We demonstrate in this paper, that the optical absorption spectroscopy is an effective tool for characterisation of the electrical properties and structure of SWCNT.

1. Introduction

SWCNT show many interesting electrical and mechanical properties and are promising candidates for e.g. high strength composite materials [1–3]. Each SWCNT has characteristic n, m numbers which describe the chirality and the electronic character of the tube. SWCNT can be seen as a single rolled up graphene sheet. The numbers n, m of a SWCNT define a vector $\mathbf{C} = n\, \mathbf{a_1} + m\, \mathbf{a_2}$ which shows the direction in which a graphene sheet needs to be rolled up in order to create the SWCNT with the chirality (n,m) (Fig. 1).

The semiconducting (sc) SWCNT can be divided in type I and type II with $(2n+m)\mathrm{mod}3 = 1$ and $(2n+m)\mathrm{mod}3 = 2$, resp. The metallic (m) SWCNT have $(2n+m)\mathrm{mod}3 = 0$. From a known (n,m)-chirality the SWCNT diameter d can be calculated using:

$$d = \frac{a\sqrt{n^2 + nm + m^2}}{\pi} \tag{1}$$

with $a = 0.246$ nm.

There are different techniques to investigate the diameter of SWCNT and chirality as electron microscopy or fluorescence spectroscopy [4,5]. Other common characterisation methods for SWCNT are optical absorption spectroscopy (OAS) and the resonant Raman spectroscopy. Using OAS, diameter distribution, purity or the rela-

tion between m- and sc-SWCNT can be assessed [6–8]. Both methods, the OAS as well as the resonant Raman spectroscopy, are attributed to inter-band transitions in SWCNT and are well studied in the last years [6,7].

The transition energy is e.g. dependent on the tube diameter d. By tight binding calculation a simple relation between nanotube diameter d and the transition energies $E_{\mathrm{sc,m}}$ of sc- and m-SWCNT was defined [1,6,7]:

$$E_{\mathrm{sc,m}} = 2i\frac{\gamma_0 a_{\mathrm{C-C}}}{d} \tag{2}$$

with $i = 1$ for S_{11}, $i = 2$ for S_{22} and $i = 3$ for M_{11}; $\gamma_0 = 2.9$ eV is the nearest neighbour carbon–carbon interaction energy and $a_{\mathrm{C-C}} = 0.144$ nm is the nearest neighbour carbon–carbon distance. $E_{\mathrm{sc,m}}$ is the energy distance between the van Hove singularities and d is the tube diameter. However, because of discrepancies with experimental results different modifications and improvements of Eq. (2) were necessary to get a more accurate calculation of $E_{\mathrm{sc,m}}$ and a better congruence with experimental results [9–12]. Saito et al. calculated the transition energy $E_{\mathrm{sc,m}}$ by taking into account the exciton binding energy E_b between the electron and the hole, the self-energy Σ and the gap energy E_g between the valence and conduction band. The different energy contributions for $E_{\mathrm{sc,m}}$ are shown in Fig. 2b. However, also the material which surrounds the SWCNT has an influence on the transition energy $E_{\mathrm{sc,m}}$ [13]. A model for ambient effects on the transition energy $E_{\mathrm{sc,m}}$ was introduced by Nugraha et al. [14]. They used for the calculation of $E_{\mathrm{sc,\underline{m}}}$ a

* Corresponding author. Tel.: +49 351 83391 3415.
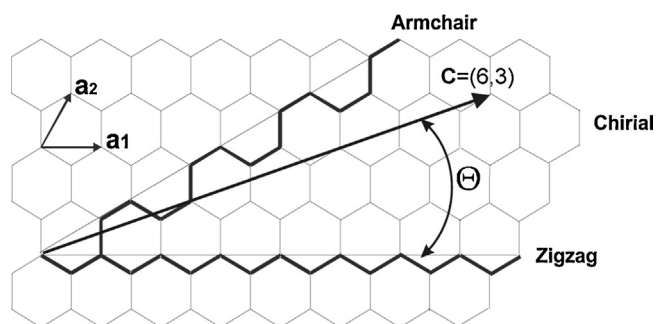 *E-mail address:* aljoscha.roch@iws.fraunhofer.de (A. Roch).

Fig. 1. The vector $C = (n\,a_1 + m\,a_2) = (6\,a_1 + 3\,a_2)$ defines a chiral SWCNT (6,3). The SWCNT with $\theta = 0$ or $30°$ are called zigzag or armchair tubes.
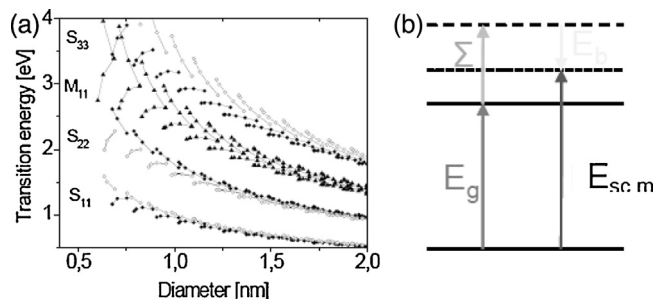

Fig. 2. (a) Kataura plot, calculated with the extended tight binding approximation and with $\kappa = 2.22$ for bundled SWCNT (data provided by Saito et al. [14,16]) The transition energies for sc-SWCNT with full circles are $(2n+m)\mathrm{mod}3 = 1$ and with empty circles are $(2n+m)\mathrm{mod}3 = 2$. (b) The different energy contributions which are responsible for the transition energy $E_{sc,m}$. E_g is the gap energy, E_b is the exciton binding energy and Σ is the self-energy.

Additionally we calculated e.g. the exciton binding energy in m-SWCNT by OAS at high temperature.

2. Experimental

SWCNT have been catalytically synthesised at 1273 K under constant conditions with a modified pulsed arc technique within a 7 m long custom-built tube furnace in nitrogen gas [17]. The setup is shown in Fig. 3. The synthesis takes place in zone 1 at 1273 K. Here, the anode is evaporated by a pulsed arc discharge. The graphite anode was doped with transition metals. During the cooling process of the evaporation plume the SWCNT grow. A more detailed description of the SWCNT synthesis process is presented in Ref. [18]. The synthesis products (35% SWCNT, 20% catalyst particles and 45% amorphous carbon) were swept downstream with an continuous gas flow of $5\,\mathrm{cm\,s^{-1}}$ and were finally collected in a gas scrubber at the end of the reactor. We synthesised a few hundred gram material per day.

Downstream, behind the 0.5 m long synthesis zone (zone 1), a 6.5 m long cooling zone (zone 2) was connected by a heat barrier to suppress any gas convection between the two zones. In the cooling zone, the tube furnace temperature was adjusted to temperatures between 373 K and 1273 K, depending on the experimental needs. At the end of the cooling zone, two side-tube connectors with windows opposite to each other were used for the in-line OAS characterisation of the aerosol stream inside the tube furnace [19]. The main advantage of this approach is that the SWCNTs were kept freely floating within the aerosol stream in the inert gas stream, thus avoiding any unwanted contributions from substrate clamping as well as contributions from adsorption and functionalisation effects from gaseous impurities like oxygen or water. Two spectrometer, the NanoSpectralyzer NS1 and the Brucker Matrix F were used to measure the metallic and semiconducting absorption bands. From the obtained 50 spectra of nanotube material at the selected temperatures, the positions of the most relevant optical SWCNT features, the S_{11} and S_{22} absorption bands for sc-SWCNTs and the M_{11} absorption band for m-SWCNTs, have been determined. The calculated mean transition energy $E_{sc,m}$ remained very close around a mean value (within a few meV) for each temperature. This provided sufficient measurement accuracy for our experiments.

3. Results and discussion

Selected in situ measured single spectra at 673 K are exemplarily shown in Fig. 4.

A detailed analysis of the averaged absorption bands at room temperature is shown in Fig. 5. The S_{11}-, S_{22}- and M_{11}-absorption bands are a superposition of contributions from many SWCNT which contribute to the absorption bands. The arrows in Fig. 5a, b and c show the energy positions where a particularly large

dielectric constant of $\kappa = 2.22$. Saito et al. calculated and provided finally the transition energies $E_{sc,m}$ for any (n,m) chirality with respect to all known parameters [14–16]. The corresponding Kataura plot is shown in Fig. 2.

We demonstrate in this paper that the values shown in Fig. 2a are on good agreement to our experimental data and that the extensive calculation of the transition energy by Saito et al. delivers very exact values. Though there are different commercial SWCNT sources available, the structure of the SWCNT products is generally not well analysed. We measured the optical absorption of the SWCNT in inert atmosphere directly after the synthesis in order to avoid side effects of adsobates [8,13] and demonstrate the analysis by OAS based on the calculation from Saito et al. Furthermore we present for the first time OAS spectra of SWCNT at high temperatures. The information from these spectra expands the information content which can be gained by OAS. We show that the detailed theoretical analysis is well suited for room temperature characterisation of SWCNT, however at higher temperature the temperature dependence of the transition energy needs to be considered.
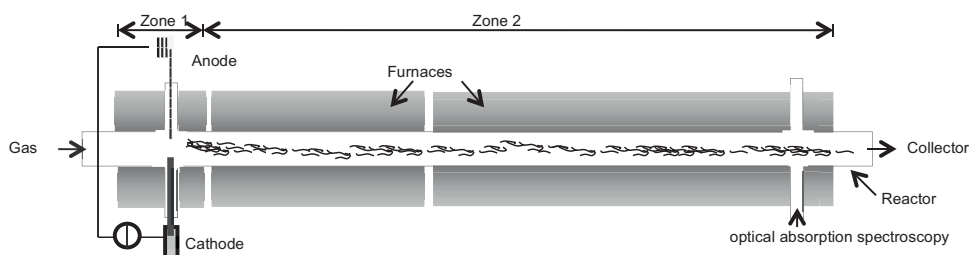

Fig. 3. In zone 1 the SWCNT synthesis takes place at 1273 K. In zone 2 the temperature was changed between 373 and 1273 K. At the end of the furnaces the optical absorption spectroscopy was done.
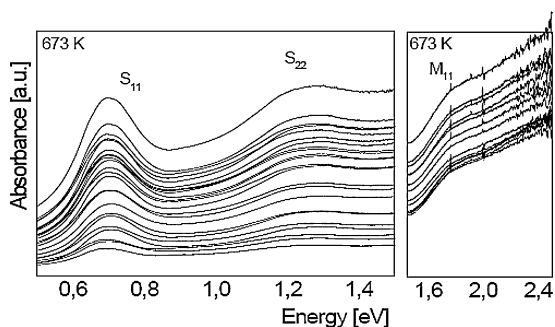
Fig. 4. OAS spectra of SWCNT aerosol in the zone 2 at 673 K. The spectra of the sc-SWCNT (S_{11}, S_{22}) were measured with the Brucker Matrix F and the spectra of the m-SWCNT (M_{11}) were measured with the NanoSpectralyzer NS1. Afterwards, the S_{11} and S_{22} as well as the M_{11} spectras were averaged.

number of SWCNT have comparable transition energies. In Fig. 5d, e and f is shown the good conformity between experiment and calculated values by the horizontal lines, indicating the position of the dominant peaks in the absorption spectra. The energy distance between two neighbouring dominant peaks corresponds quite well to the calculated energy position in the Kataura plot.

From the spectra of the sc-SWCNT the diameter of the sc-SWNCT can be determined with $d \approx 1.0$–1.75 nm. By the same way the diameter of the m-SWCNT can be determined with $d \approx 1.1$–1.7 nm. The sub bands of the M_{11}-band have the largest energy dis-

tances and strongest splitting in the absorption spectra. This is comparable to the energy branches in the Kataura plot of the m-SWCNT. The sc-SWNCT have a less clear energy splitting and therefore the sub band position is closer, more overlapping and for the S_{11} just weakly. The absorption bands (S_{11}, S_{22} and M_{11}) were approximated with up to 6 Gauss curves with a half-value width of 0.05–0.15 eV (Fig. 5). The comparison of the measured spectra with the calculated data by Saito et al. showing good accordance.

The chiralities (n,m) of the SWCNTs which can be produced by the pulsed arc can be determined by OAS as shown in Table 1.

The spectra, determined by averaging all of the in situ OAS spectra at different furnace temperatures, are shown in Fig. 6 after background subtraction. With increasing furnace temperature the band position of the S_{11}-, S_{22}-, and M_{11}-band shifts to lower energies. A comparable effect was shown by resonant Raman spectroscopy [20,21]. The small figures in Fig. 6 show background subtracted spectra without normalisation. For the m-SWCNT and the M_{11}-band respectively, a relative change in the intensities of the absorption band with increasing temperature was observed. The reason of this effect is not analysed here and needs further investigations.

The Varshni-equation describes the dependence of the band gap energy E_g on the temperature [22]. By fitting the shift of the transition energy with the Varshni-equation we found that the Varshni-equation is in accordance with the experimental data. The shift of the mean transition energy $E_{sc,m}(T)$ follows the
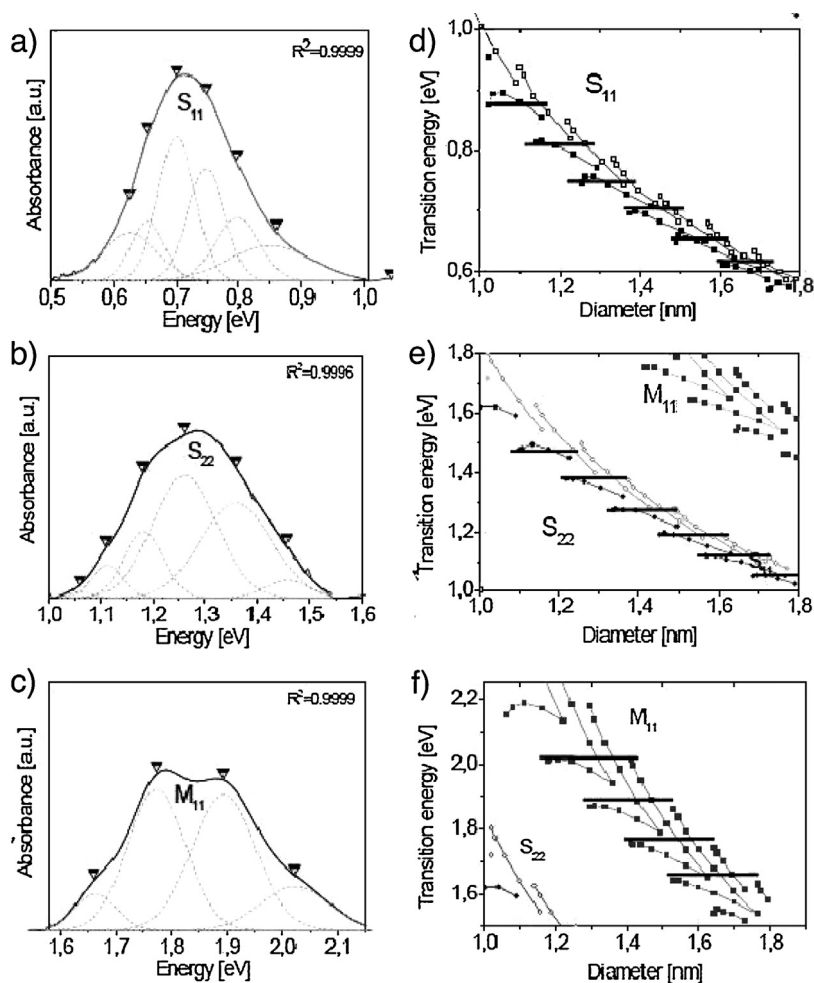

Fig. 5. (a–c) S_{11}-, S_{22}- and M_{11}-absorption bands and approximated curve fitting by multiple Gauss curves. (d–f) Comparison of Gauss curve position with the calculated Kataura plot. The half-value width of the fitting curves vary between ~0.05 and 0.15 eV.
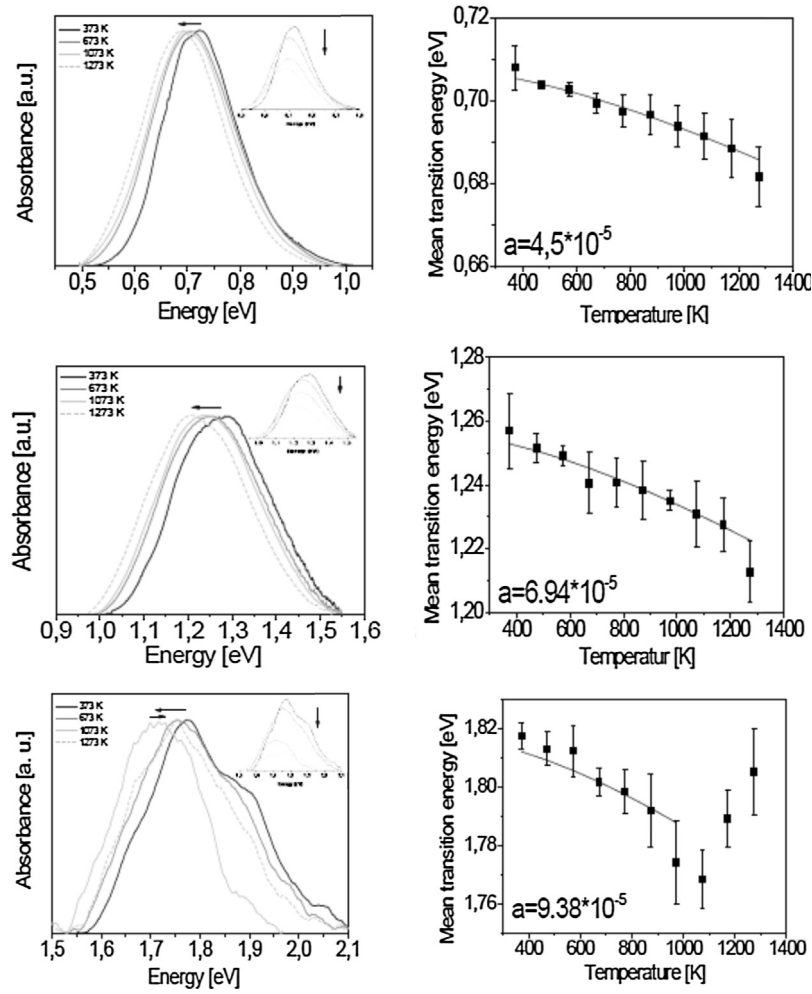
Fig. 6. (left) Sub ground subtracted in situ absorbance bands (S_{11}, S_{22} and M_{11}) of SWCNT-clouds swapping through the furnace at different temperatures (373–1273 K). The spectra are normalised to show the shift of the band position. The small figures show non normalised spectra. These small figures demonstrate the relative loss of the band area with increasing temperature. (right) Energy positions of the averaged bands at different temperatures. The positions were determined by Gauss approximations and the error bars are the uncertainty of these approximations, specified by the calculation programme. a is the fitting parameter of Eq. (3).

Varshni-equation, if the specific material parameters a and b are defined as shown below and mentioned in Fig. 6 (right):

$$E_g(T) = E_0 - \frac{aT^2}{T+b} \tag{3}$$

E_0 is the energy for $E_g(T=0)$ and a and b are constants. T is the temperature.

If we replace the $E_g(T)$ with $E_{sc,m}(T)$ and assume $E_0 \approx E_{sc,m}(T=373 \text{ K})$, the Varshni-equation can be used as an approximation of the shift of the mean transition energy $E_{sc,m}(T)$ (Fig. 6 (right)). The constant b can be replaced by the Debye temperature of the material as proposed by Varshni (for SWCNT ~ 2000 K [3]).

The shift can be attributed to the temperature dependence of lattice dilatation and the relative shift of the conductance and valence band due to the electron lattice interaction. About 25% of the energy shift can be attributed to the lattice dilatation [22].

The change of the transition energy $E_{sc,m}(T)$ between 373–1273 K and 373–973 K for the sc- and m-SWCNT can be calculated by deriving Eq. (3) and averaging over the temperature range.

$$\frac{dE_{11}^S}{dT} \approx -2.17 \cdot 10^{-5} \left[\frac{eV}{K} \right] \tag{4}$$

$$\frac{dE_{22}^S}{dT} \approx -3.35 \cdot 10^{-5} \left[\frac{eV}{K} \right] \tag{5}$$

$$\frac{dE_{11}^M}{dT} \approx -4.04 \cdot 10^{-5} \left[\frac{eV}{K} \right]$$

The transition energy of the m-SWCNT follows also the Varshni-equation. This is in accordance with inter band transition in m-SWCNT and the existence of excitons in m-SWCNT. In solids, apart from semiconductors, excitons can hardly exist, however, modulation shows that in m-SWCNT excitons are possible.

At higher temperatures the mean transition energy of m-SWCNT shifts back to higher energies. This indicates the exceeding of the exciton binding energy. Excitons can exist as long as the equation ($E_b \leq kT$) holds.

The theoretical binding energies E_b of excitons in m-SWCNT are determined with 50–100 meV by modelling [23–25]. Experimental results on m-SWCNT, with resonant Raman spectroscopy, have shown an exciton binding energy of $E_b \approx 50$ meV [26]. The average binding energy E_b of excitons in m-SWCNT with diameters between 1.1 and 1.7 nm can be determined with 80–90 meV. The exciton binding energy of the sc-SWCNT is between 400 and 1000 meV [24,27] and therefore not measurable with our setup. The temperature needs to be increased up to >4000 K to measure a blue shift for the S_{11} or S_{22} band.

Table 1
Chiralities of SWCNT produced by pulsed arc technique. The data are based on the values in Fig. 5 d–f. It is not possible to give the exact chirality distribution by the OAS, however the bold labelled values are the dominate chiralities in the OAS and therefore the preferential synthesised chiralities.

sc-SWCNT-Type I					sc-SWCNT-Type II					m-SWCNT				
(n,m)	$2n+m$	d [nm]	E_{11} [eV]	E_{22} [eV]	(n,m)	$2n+m$	d [nm]	E_{11} [eV]	E_{22} [eV]	(n,m)	$2n+m$	d [nm]	E_{11L} [eV]	E_{22H} [eV]
(9,7)	25	1.091	0.912	1.593	(8,7)	23	1.021	0.954	1.720	(8,8)	24	1.088	2.352	2.352
(10,5)	25	1.039	0.964	1.621						(9,6)	24	1.027	2.390	2.556
(11,3)	25	1.004	1.006	1.620	(9,8)	26	1.156	0.855	1.545					
(12,1)	25	0.986	1.035	1.607	(10,6)	26	1.099	0.882	1.641	(9,9)	27	1.223	2.133	2.133
					(11,4)	26	1.057	0.896	1.718	(10,7)	27	1.161	2.173	2.283
(10,8)	28	1.225	0.820	1.450	(12,2)	26	1.030	0.894	1.775	(11,5)	27	1.113	2.189	2.431
(11,6)	28	1.172	0.862	1.479	(13,0)	26	1.022	0.876	1.803	(12,3)	27	1.080	2.176	2.557
(12,4)	28	1.132	0.891	1.495						(13,1)	27	1.063	2.154	2.635
(13,2)	28	1.108	0.926	1.482	**(10,9)**	**29**	**1.291**	**0.772**	**1.398**					
(14,0)	28	1.100	0.937	1.477	(11,7)	29	1.233	0.794	1.479	**(10,10)**	**30**	**1.358**	**1.940**	1.940
					(12,5)	29	1.187	0.809	1.544	**(11,8)**	**30**	**1.295**	**1.983**	2.064
(11,9)	**31**	**1.360**	**0.745**	**1.320**	(13,3)	29	1.156	0.816	1.595	**(12,6)**	**30**	**1.245**	**2.010**	2.184
(12,7)	**31**	**1.305**	**0.782**	**1.350**	(14,1)	29	1.140	0.813	1.625	**(13,4)**	**30**	**1.208**	**2.016**	2.286
(13,5)	**31**	**1.262**	**0.811**	**1.369**						**(14,2)**	**30**	**1.185**	**2.016**	2.362
(14,3)	31	1.233	0.834	1.377	**(11,10)**	**32**	**1.426**	**0.707**	**1.282**	**(15,0)**	**30**	**1.177**	**2.009**	2.394
(15,1)	31	1.218	0.848	1.379	**(12,8)**	**32**	**1.366**	**0.728**	**1.346**					
					(13,6)	**32**	**1.319**	**0.745**	**1.402**	(11,11)	33	1.493	1.788	1.788
(12,10)	**34**	**1.495**	**0.683**	**1.220**	(14,4)	32	1.284	0.757	1.445	(12,9)	33	1.430	1.828	1.885
(13,8)	**34**	**1.438**	**0.713**	**1.249**	(15,2)	32	1.262	0.756	1.479	(13,7)	33	1.378	1.857	1.984
(14,6)	**34**	**1.393**	**0.733**	**1.272**	(16,0)	32	1.255	0.746	1.499	(14,5)	33	1.337	1.869	2.066
(15,4)	**34**	**1.360**	**0.761**	**1.274**						(15,3)	33	1.310	1.871	2.140
(16,2)	**34**	**1.340**	**0.777**	**1.278**	**(12,11)**	**35**	**1.561**	**0.650**	**1.180**	(16,1)	33	1.296	1.869	2.180
(17,0)	**34**	**1.333**	**0.787**	**1.273**	**(13,9)**	**35**	**1.501**	**0.667**	**1.236**					
					(14,7)	35	1.451	0.682	1.285	(12,12)	36	1.628	1.650	1.650
(13,11)	37	1.629	0.631	1.126	**(15,5)**	**35**	**1.413**	**0.694**	**1.322**	(13,10)	36	1.565	1.687	1.735
(14,9)	37	1.572	0.658	1.152	**(16,3)**	**35**	**1.387**	**0.700**	**1.353**	(14,8)	36	1.511	1.719	1.818
(15,7)	**37**	**1.525**	**0.680**	**1.175**	**(17,1)**	**35**	**1.373**	**0.696**	**1.374**	(15,6)	36	1.468	1.739	1.890
(16,5)	**37**	**1.489**	**0.697**	**1.191**						(16,4)	36	1.437	1.753	1.950
(17,3)	**37**	**1.464**	**0.712**	**1.198**	(13,12)	38	1.696	0.604	1.098	(17,2)	36	1.417	1.753	1.995
(18,1)	**37**	**1.452**	**0.724**	**1.192**	(14,10)	38	1.635	0.620	1.144	(18,0)	36	1.411	1.755	2.015
					(15,8)	38	1.584	0.635	1.185					
(14,12)	40	1.764	0.587	1.052	(16,6)	38	1.543	0.649	1.217	**(13,13)**	**39**	**1.763**	**1.539**	1.539
(15,10)	40	1.706	0.610	1.078	(17,4)	38	1.513	0.655	1.246	**(14,11)**	**39**	**1.699**	**1.575**	1.608
(16,8)	40	1.658	0.626	1.100	(18,2)	38	1.495	0.660	1.266	**(15,9)**	**39**	**1.644**	**1.602**	1.679
(17,6)	40	1.618	0.646	1.108	(19,0)	38	1.489	0.646	1.280	(16,7)	39	1.599	1.620	1.737
(18,4)	40	1.590	0.660	1.118						(17,5)	39	1.565	1.634	1.793
(19,2)	40	1.573	0.675	1.118	16,9	41	1.717	0.587	1.102	(18,3)	39	1.541	1.641	1.837
(20,0)	40	1.567	0.681	1.121	17,7	41	1.674	0.600	1.131	(19,1)	39	1.529	1.643	1.863
					18,5	41	1.641	0.609	1.157					
(17,9)	43	1.790	0.587	1.024	19,3	41	1.618	0.610	1.179	**17,8**	**42**	**1.731**	**1.518**	1.615
(18,7)	43	1.749	0.599	1.042	20,1	41	1.607	0.611	1.191	**18,6**	**42**	**1.694**	**1.538**	1.659
(19,5)	43	1.717	0.612	1.054						**19,4**	**42**	**1.667**	**1.546**	1.700
(20,3)	43	1.696	0.624	1.054	19,6	44	1.770	0.574	1.077	**20,2**	**42**	**1.650**	**1.552**	1.727
(21,1)	43	1.685	0.633	1.052	20,4	44	1.744	0.581	1.095	(21,0)	42	1.645	1.540	1.741
					21,2	44	1.728	0.571	1.114					
					22,0	44	1.723	0.568	1.123	(20,5)	45	1.794	1.454	1.582
										(21,3)	45	1.773	1.462	1.610
										(22,1)	45	1.763	1.462	1.630

Besides the band position also the relative band intensities/area change with increasing temperature. The band intensity of the first transitions are strongly influenced by the temperature and become smaller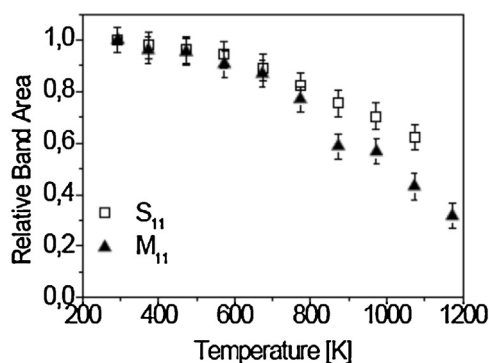 with increasing temperature as shown in Fig. 7. With increasing temperature the exciton lifetime decreases in SWCNT [28] and this explains the decreasing absorption intensity.

4. Conclusion

We have shown that the transition energies in SWCNTs become smaller with increasing temperature. The change in the transition energy follows the Varshni-equation. The band intensity/area is also influenced by the temperature and becomes smaller with increasing temperature. The blue shift of the M_{11} band above 973 K can be explained by exciton dissociation. We calculated the mean exciton binding energy of m-SWCNT with ∼80–90 meV.

Fig. 7. Relative band intensity of the S_{11}-, and M_{11}-band with increasing temperature.

References

[1] R. Saito, G. Dresselhaus, M.S. Dresselhaus, Physical Properties of Carbon Nanotubes, Imperial College Press, London, 2001.
[2] J. Ali, Guo Jing, P. Magnus, Wang Qian, D. Mann, M. Lundstrom, Hongjie Dai, Phys. Rev. Lett. 92 (2004) 106804.
[3] Zhen Yao, C.L. Kane, C. Dekker, Phys. Rev. Lett. 84 (2000) 2941–2944.
[4] E.T. Thostenson, Chunyu Li, Tsu-Wei Chou, Compos. Sci. Technol. 65 (2005) 491–516.
[5] S.M. Bachilo, M.S. Strano, C. Kittrell, R.H. Hauge, R.E. Smalley, R.B. Weisman, Science 298 (2002) 2361–2366.
[6] H. Katauraa, Y. Kumazawaa, Y. Maniwaa, I. Umezub, S. Suzukic, Y. Ohtsukac, Y. Achiba, Synth. Met. 103 (1999) 2555–2558.
[7] X. Liu, T. Pichler, M. Knupfer, M.S. Golden, J. Fink, H. Kataura, Y. Achiba, Phys. Rev. B 66 (2002) 045411.
[8] M.E. Itkis, D.E. Perea, S. Niyogi, S.M. Rickard, M.A. Hamon, H. Hu, B. Zhao, R.C. Haddon, Nano Lett. 3 (2003) 309–314.
[9] R.B. Weisman, S.M. Bachilo, Nano Lett. 3 (2003) 1235–1238.
[10] G. Dukovic, F. Wang, D. Song, M.Y. Sfeir, T.F. Heinz, L.E. Brus, Nano Lett. 5 (2005) 2314–2318.
[11] A. Jorio, P.T. Araujo, S.K. Doorn, S. Maruyama, H. Chacham, M.A. Pimenta, Phys. Status Solidi B 243 (2006) 3117–3121.
[12] J. Jiang, R. Saito, Ge.G. Samsonidze, A. Jorio, S.G. Chou, G. Dresselhaus, M.S. Dresselhaus, Phys. Rev. B 75 (2007) 035407.
[13] C. Fantini, A. Jorio, M. Souza, M.S. Strano, M.S. Dresselhaus, M.A. Pimenta, Phys. Rev. Lett. 93 (2004) 147406.
[14] A.R.T. Nugraha, R. Saito, K. Sato, P.T. Araujo, A. Jorio, M.S. Dresselhaus, Appl. Phys. Lett. 97 (2010) 091905.
[15] K. Sato, R. Saito, J. Jiang, G. Dresselhaus, M.S. Dresselhausd, Vib. Spectrosc. 45 (2007) 89–94.
[16] K. Sato, R. Saito, J. Jiang, G. Dresselhaus, M.S. Dresselhaus, Phys. Rev. B 76 (2007) 195446.
[17] A. Roch, M. Märcz, U. Richter, A. Leson, E. Beyer, O. Jost, Phys. Status. Solidi B 246 (2009) 2511–2513.
[18] A. Roch, O. Jost, B. Schultrich, E. Beyer, Phys. Status Solidi B 244 (2007) 3907–3910.
[19] (a) M. Leistner, Optisch-spektroskopische Untersuchungen zur Optimierung des Herstellungsprozesses von Single Wall Carbon Nanotubes (Master Thesis), TU Dresden, 2009;
(b) M. Leistner, In-situ-Monitoring des Syntheseprozesses einwandiger Carbon-Nanotubes durch Nahinfrarotspektroskopie, 63, Fraunhofer IWS Jahresbericht, 2007, 2008.
[20] S.N. Bokova, V.I. Konov, E.D. Obraztsova, A.V. Osadchii, A.S. Pozharov, S.V. Terekhov, Quantum Electron. 33 (7) (2003) 645–650.
[21] E.D. Obraztsova, V.Yu. Yurov, V.M. Shevluga, R.E. Baranovsky, V.A. Nalimova, V.L. Kuznetsov, V.I. Zaikovskii, Nanostruct. Mater. 11 (3) (1999) 295–306.
[22] Y.P. Varshni, Physica 34 (1967) 149–154.
[23] J. Deslippe, C.D. Spataru, D. Prendergast, S.G. Louie, Nano Lett. 7 (2007) 1626–1630.
[24] C.D. Spataru, S. Ismail-Beigi, L.X. Benedict, S.G. Louie, Phys. Rev. Lett. 92 (2004) 077402.
[25] F. Wang, D.J. Cho, B. Kessler, J. Deslippe, P.J. Schuck, S.G. Louie, A. Zettl, T.F. Heinz, Y.R. Shen, Phys. Rev. Lett. 99 (2007) 227401.
[26] P. May, H. Telg, G. Zhong, J. Robertson, C. Thomsen, J. Maultzsch, Phys. Rev. B 82 (2010) 195412.
[27] F. Wang, G. Dukovic, L.E. Brus, T.F. Heinz, Sci. Rep. 308 (2005) 838–841.
[28] A. Hagen, M. Steiner, M.B. Raschke, C. Lienau, T. Hertel, H. Qian, A.J. Meixner, A. Hartschuh, Phys. Rev. Lett. 95 (2005) 197401.